Proton beam electron return effect: Monte Carlo simulations and experimental verification

Lühr, A.; Burigo, L. N.; Gantz, S.; Schellhammer, S.; Hoffmann, A. L.;

Originally published:

January 2019

Physics in Medicine and Biology 64(2019)3, 035012

DOI: https://doi.org/10.1088/1361-6560/aafab4

Magnetic field-induced proton dose enhancement: Monte Carlo simulations and experimental verification

A. Lühr[1,2,3,*], L.N. Burigo[4,5,*], S. Gantz[1,2], S.M. Schellhammer[1,2], A.L. Hoffmann[1,2,6].

[1]Helmholtz-Zentrum Dresden - Rossendorf, Institute of Radiooncology – OncoRay, Dresden, Germany.
[2]OncoRay - National Center for Radiation Research in Oncology, Faculty of Medicine and University Hospital Carl Gustav Carus, Technische Universität Dresden, Helmholtz-Zentrum Dresden - Rossendorf, Dresden, Germany.
[3]German Cancer Consortium (DKTK), Partner Site Dresden, Dresden, Germany.
[4]German Cancer Research Center DKFZ, Division of Medical Physics in Radiation Oncology, Heidelberg, Germany.
[5]National Center for Radiation Research in Oncology NCRO, Heidelberg Institute for Radiation Oncology HIRO, Heidelberg, Germany.
[6]Department of Radiotherapy and Radiation Oncology, Faculty of Medicine and University Hospital Carl Gustav Carus, Technische Universität Dresden, Dresden, Germany.

[*] Both authors contributed equally to this work

Abstract

Introduction

Proton therapy is expected to benefit from integration with magnetic resonance (MR) imaging. However, the magnetic field distorts the dose distribution and induces a local dose enhancement at tissue-air interfaces by the electron return effect (ERE). For MR-integrated X-ray therapy (MRXT), a dose enhancement ratio (DER) up to 40% compared to no magnetic field has been reported. The objective of this study was to provide experimental evidence for the ERE in proton beams in a transverse magnetic field and to systematically characterise the dependence of the DER on magnetic field strength, orientation as well as proton beam energy and voxel size by computer simulations.

Methods

EBT3 films were irradiated with 200 MeV protons with and without a 0.92 T transverse field of a permanent magnet. Films with an effective measurement depth of 0.156 and 0.467 mm were either (A) sandwiched between two PMMA slabs of 10 mm thickness or (B) attached to the distal face of one PMMA slab. The dose measured in setup (B) was normalised to the dose in the reference setup (B) without air interface. Reference conditions (A) were also used to determine the proton dose response of EBT3 films with and without magnetic field. High-resolution Monte Carlo simulations were performed to reproduce the irradiation experiments and to calculate the DER for proton energies between 50–200 MeV and magnetic field strengths between 0.35–3 T as function of distance from the air interface. Voxel sizes of 0.05, 0.5 and 1 mm were analysed.

Results

EBT3 films showed a significant under-response of about 3% in the magnetic field. DERs of (2.2 ± 0.4)% and (0.5 ± 0.6)% were measured at 0.156 and 0.467 mm from the air interface, respectively. Measurements and simulations agreed within 0.15%. For a 200 MeV proton beam, the DER in a 0.05 mm voxel at the interface increased with magnetic field strength from 2.6% up to 8.2% between 0.35 and 1.5 T,

respectively. For a 1.0 T magnetic field, the DER increased from 3.2% up to 7.6% between 50 and 200 MeV, respectively. For voxel sizes of 0.5 and 1 mm, the maximum calculated DER decreased to 2.6% and 1.4%, respectively.

Conclusion

The ERE for proton beams in transverse magnetic fields is measurable. The local dose enhancement is well predictable, decreases rapidly with distance from the air interface, and is negligible beyond 1 mm depth. Although the ERE is much smaller than for MRXT, its impact cannot be ignored for air-filled ionisation chambers and for porous tissues (e.g. lung parenchyma) being irradiated with proton beams in the presence of a magnetic field.

1. **Introduction**

In recent years, there has been a strong increase in the interest for proton therapy (PT). This is because of the unique depth-dose characteristics, which can be exploited to achieve significant reductions in normal-tissue dose proximal and distal to the tumour volume. While this holds the potential for reducing the risk of treatment-related side-effects and the induction of secondary neoplasms, PT is more susceptible to morphological changes (i.e. anatomical deformations and organ motion) and patient set-up uncertainties than high-energy X-ray therapy. One approach to improve the targeting accuracy for moving targets is by tracking the anatomical changes during dose delivery with real-time magnetic resonance (MR) imaging. MR offers high-resolution imaging with unmatched soft-tissue contrast in the absence of ionizing radiation. MR-integrated X-ray therapy (MRXT) has become clinically available since 2014 with the introduction of the ViewRay MRIdian system, consisting of a 0.35 T split-bore MRI scanner coupled with a three-head ^{60}Co radiation source (Mutic and Dempsey 2014). Recently, the first patients were treated on the Elekta Unity MR-LINAC system, consisting of a closed-bore 1.5 T MRI scanner coupled with a 7 MV linear accelerator (Raaymakers *et al* 2017).

As a next step in the technological development of image-guided radiation therapy, the concept of combining real-time MR image guidance with PT has gained interest from the scientific community during the past years (Oborn *et al* 2017a). Targeting accuracy of PT is expected to benefit even more from MR-guidance than X-ray therapy. Dose distributions with steep gradients and typically few beam directions make PT more sensitive to anatomical variations than X-ray therapy. Merging MR imaging and PT would provide an opportunity to fully exploit the dosimetric benefit of PT and realise its clinical potential.

However, the integration of MR imaging and PT imposes several technical challenges due to mutual electromagnetic interactions between the proton beam delivery system and the MR scanner. Firstly, the static magnetic field of the MR scanner affects the trajectory of charged particles, which results in a distorted dose distribution. Simulation studies for transverse magnetic fields showed that the proton beam is deflected and the Bragg peak position is displaced laterally by a few millimetres up to some centimetres, depending on the magnetic field strength and the initial proton

beam energy (Schellhammer and Hoffmann 2017, Moteabbed *et al* 2014, Fuchs *et al* 2017, Raaymakers *et al* 2008). The deflection of a proton beam slowing down in homogeneous media is well predictable as has recently been confirmed experimentally for the first time (Schellhammer *et al* 2018).

In addition, the static magnetic field can also cause local dose enhancements in heterogeneous tissue geometries where a lower density medium is distal to a higher density medium, for example at tissue-air interfaces in lung parenchyma. Here, secondary electrons scattered in the lower density medium may have a sufficiently large range to return to the originating high-density medium under the influence of the Lorentz force. This effect, known as the electron return effect (ERE), has been observed in MRXT with a reported dose enhancement of up to 40% at tissue-air interfaces in strong transverse magnetic fields (Raaijmakers *et al* 2005, 2008).

For MRPT, the effect is expected to be smaller than for MRXT due to the substantially lower kinetic energy of secondary electrons in PT. However, no consensus on the magnitude of the ERE exists in the scarcely available literature. From the very few simulation studies published, estimates range from no effect (Raaymakers *et al* 2008) to a dose enhancement of about 2% (Fuchs *et al* 2017) depending on the parameters considered in the simulations. A major shortcoming of the available literature is that neither experimental data nor a systematic study on the impact of relevant parameters on the ERE, such as magnetic field strength and proton beam energy, have been reported yet. Therefore, the main objectives of this study were 1) to experimentally confirm the existence of the ERE for PT by measurements and 2) to determine its magnitude for clinically relevant proton energies, magnetic field strengths, and magnetic field orientations using Monte Carlo particle transport simulations.

2. Material and Methods

2.1. Irradiation experiment

All experiments were carried out at the horizontal research beam line in the experimental room at our proton therapy facility. The measurement setup is depicted

in Figure 1. It consists of a collimated proton beam, a slab phantom containing vertically oriented film dosimeters, and a permanent magnet assembly.

2.1.1. Experimental setup

A 216.9 MeV proton beam having an energy spread (one sigma) of 1.3 MeV at the beam exit was used in all measurements. A Bragg peak ionisation chamber (TM34070, PTW, Freiburg) and a scatterer slab of PMMA were placed at 88.5 mm downstream from the beam exit as independent monitor chamber and to increase the lateral dose uniformity at the measurement position, respectively. The combined PMMA-equivalent thickness of the scatterer and the chamber is about 31 mm, reducing the proton energy to approximately 200 MeV at the entrance of a target phantom, which was located 1448 mm downstream of the beam exit inside the magnetic field produced by a C-shaped magnet assembly. A cylindrical brass collimator (outer diameter 180 mm, thickness 66 mm) with a central 12 mm diameter opening was positioned 1000 mm downstream of the PMMA slab to minimise unintended radiation exposure to the magnet assembly and to produce a circular beam profile with an approximately homogeneous dose distribution in its central region.

The collimated 200 MeV proton beam traversed a target phantom consisting of either one or two 10 mm thick slabs of PMMA. The front face of the proximal slab was placed 301.5 mm downstream of the collimator. Dose was measured with GAFChromic™ EBT3 films (Ashland, Covington, USA; PMMA-equivalent thickness of 0.312 mm (Beyreuther 2018)) using two experimental setups:

(A) Reference conditions: one film was sandwiched between the proximal and distal PMMA slab of 10 mm thickness each. This setup was used for dose normalization with and without magnetic field since no ERE is expected under these conditions.

(B) Measurement conditions: two films were attached to the distal side of the 10 mm thick proximal PMMA slab and no distal PMMA slab was used. In this setup, electrons travelling in the air distally from the PMMA-air interface may return to the PMMA slab in the presence of a magnetic field and deposit their energy in the films.

The fluence and the energy of the proton beam at the point of measurement were considered identical in both setups (A) and (B). The EBT3 film was comprised of a 0.028 mm active layer sandwiched between two 0.125 mm matte-polyester substrates. The centre of the film (at 0.156 mm PMMA-equivalent thickness) was considered as the effective measurement point. For setup (B), two EBT3 films were attached to the proximal PMMA slab within the magnet resulting in measurements at two PMMA-equivalent effective depths from the PMMA-air interface: 0.156 mm and 0.467 mm. For setup (B) without magnet, only one EBT3 film was used with an effective measurement depths from the PMMA-air interface of 0.156 mm. While the measurement position of the EBT3 film in setup (A) was practically the same as in setup (B), the distal PMMA slab increased the effective depth from the PMMA-air interface by 10 mm resulting in 10.156 mm.

For each irradiation experiment, the same number of monitor units (MU) at beam exit was used. Films were irradiated with approximately 8 Gy to ensure a good signal to background ratio as well as a linear dose response of the films. The integral dose of each film irradiation was monitored with the Bragg peak chamber to reduce the impact of possible dose fluctuations. The variation in applied dose between the irradiation of the different films was small (standard deviation of 0.15%). To eliminate the variation in applied dose, each film measurement was normalised by the corresponding Bragg peak chamber signal.

Film irradiations were performed under the same conditions without and within a transversal (vertical) magnetic field. The magnetic field was provided by a C-shaped 0.95 T permanent $Nd_2Fe_{14}B$ dipole magnet with a horizontal extension of 200 × 100 mm^2 and a vertical gap of 39 mm between the magnet poles. The central and magnetic fringe fields were characterised by 3D automated Hall probe magnetometry (Schellhammer *et al* 2018, Gantz 2017). Finite-element modelling of the magnetic field (COMSOL Multiphysics®, COMSOL AB, Stockholm, Sweden) reproduced the magnetometry results within 2% (cf. Supplement Figure 8) and was used to generate a 3D magnetic field map. The magnetic flux density at the position of the film measurements was (0.92 ± 0.02) T for setup (A) and (B).

2.1.2. Dose evaluation

Sheets of EBT3 film were cut into rectangular 90 × 37 mm^2 pieces and tightly attached to the phantom to avoid air pockets between the film and PMMA slab. The orientation of the films was kept the same for all ERE experiment, with the predominant monomer orientation, i.e. the short film side, being parallel to the magnetic field direction. After irradiation, the optical density distribution of the EBT3 films was measured by a flat-bed scanner (Expression 11000XL, Epson, Long Beach, USA) and the deposited dose distribution was analysed according to the protocol described in (Schellhammer *et al* 2018, Gantz 2017). To reduce the influence of the spatial variability in scanner and film response, the dose background of each film piece was determined as the average of the mean signal of two adjacent unirradiated 37 × 22 mm^2 film pieces. The beam centre of the measured circular beam profiles (cf. Supplement Figure 9) was determined as the position of the maximum of a bivariate Gaussian function fit applied to the measured dose distribution. The dose value measured for each irradiation experiment was defined as the average dose over a circular disk of 2.5 mm radius centred at the beam centre.

Magnetic field effects on film dosimetry

Prior to the ERE measurements, an evaluation of the EBT3 film dose response to proton irradiation in a magnetic field was performed. It was tested whether the dose response changes, first, due to a magnetic field as reported by (Delfs *et al* 2018) for photon irradiation and, second, due to the orientation of the EBT3 film monomeres relative to the magnetic field, as has been reported for GAFChromic™ EBT2 films by (Reynoso *et al* 2016). For this purpose, an experimental setup comparable to the reference condition (A) was used to ensure secondary electron equilibrium at the point of measurement. All films were placed perpendicular to the proton beam and either irradiated with or without the magnet in place. The films were orientated with their short side either parallel or perpendicular to the vertical magnetic field. Films were irradiated with different MU in a dose range from 1 to 11 Gy. Linear regression was used to generate dose response curves as function of MU.

Definition of normalised dose and dose enhancement ratio

For setup (A), it was assumed that at the effective measurement point secondary electron equilibrium existed. Furthermore, it was assumed that the dose at this point was not influenced by the ERE (as confirmed by simulations, cf. Supplement Figure 10) since the distal PMMA slab was much thicker than the maximum range of the secondary electrons. Accordingly, the dose $D_{\mathrm{A}}(B)$ obtained with setup (A) at a magnetic field strength B was considered as reference for the dose $D_{\mathrm{B}}(B)$ measured with setup (B) at the same field strength. Hence, the normalised dose was defined as the ratio of the dose measured with ERE relative to the dose without ERE,

$$D_{\mathrm{N}}(B) = \frac{D_{\mathrm{B}}(B)}{D_{\mathrm{A}}(B)}, \tag{1}$$

to minimise the influence of a possible different dose response of the EBT3 films due to the magnetic field. To quantify the ERE the dose enhancement ratio (DER) was defined as the ratio of the normalised dose with magnetic field and the normalised dose without magnetic field (i.e. $B = 0$),

$$\mathrm{DER}(B) = \frac{D_{\mathrm{N}}(B)}{D_{\mathrm{N}}(0)} = \frac{D_{\mathrm{B}}(B)}{D_{\mathrm{B}}(0)} \frac{D_{\mathrm{A}}(0)}{D_{\mathrm{A}}(B)}, \tag{2}$$

at the same effective measurement depth (i.e. the same distance to the PMMA-air interface). The second factor, $D_{\mathrm{A}}(0)/D_{\mathrm{A}}(B)$, in Eq. (2) accounts for possible small systematic differences that occurred between experiments with and without magnetic field, e.g., in the dose response of the EBT3 films, in the setup, and in the proton energy spectra.

All film irradiations were repeated such that 3 to 8 films for each measurement setup were available for analysis. The mean dose value for each setup was used to determine the normalised dose and DER as defined in Eqs. (1) and (2). The entire experiment was performed twice – denoted as experiment run Exp1 and Exp2. In total, 55 irradiated films were analysed. For a direct comparison to computer simulations, measured data from experiment run Exp1 and Exp2 were also pooled for each setup to increase the statistical power. For the comparison of the normalised doses with and without magnetic field and the DERs at different effective depths,

two-sided *t*-tests were used and *p*-values < 0.05 were considered statistically significant.

2.2. Computer simulations

Monte Carlo particle transport simulations were used to reproduce the results of the experimental measurements and to investigate the dependence of the proton dose enhancement effects on the magnetic field strength and orientation, as well as on the proton energy at the PMMA-air interface. The Monte Carlo simulations were performed using TOPAS (Perl *et al* 2012) version 3.1 based on Geant4 toolkit version 10.3 with patch 1 (Allison *et al* 2006, Agostinelli *et al* 2003).

2.2.1 Simulation of irradiation experiment

The simulation of the experimental measurements was performed in two steps to improve computational performance. Firstly, the transport of 10^7 protons of 216.9 MeV (one sigma energy spread of 1.16 MeV) from the beam exit traversing the beam line was simulated to record the energy spectrum of protons downstream of the collimator (Figure 1). The in-beam components, including scatterers and collimator were modelled according to their geometrical and material specifications. The energy spectrum at the collimator was fitted to a Gaussian function with a mean energy of 200.7 MeV and a standard deviation of 1.33 MeV. No effect of the magnetic field on the proton energy downstream of the collimator was observed.

Secondly, 10^8 primary protons downstream of the collimator were transported through the target volumes. In analogy to the experimental setup, the simulations resembled the four irradiation scenarios, comprising the combination of the two phantom setups (A) and (B) and the two magnetic field configurations (i.e., with and without magnetic field). The 3D magnetic field map produced by finite-element modelling vectors was used as input for the Monte Carlo simulations. The field map extended from the centre of the magnet up to 500 mm upstream and 200 mm downstream, thereby encompassing the region of the collimator and the phantom.

The 0.278 mm thick EBT3 films were modelled by a PMMA-equivalent layer of 0.311 mm thickness, allowing for direct calculation of the effect in PMMA without any uncertainties in the modelling of the film. The energy threshold for the production

of secondary electrons was set to 990 eV in air and 18.2 keV in PMMA (corresponding to a cut in range of 10 µm). For the analysis of the DER, the dose in the proximal PMMA slab was scored in a cuboid volume proximal to the distal edge of the film, i.e., in a region ending either at the beginning of the distal PMMA slab or at the PMMA-air interface in setup (A) and (B), respectively. The scoring volume was simulated by a 1 mm thick cuboid having a 20 × 20 mm^2 transversal cross-section, that was spatially divided into 100 bins in depth and 200 × 200 bins in the transversal plane in order to score depth-dependent 2D dose distributions.

At each depth, the 2D dose distribution of the transversal plane was obtained by averaging the 2D distributions in five consecutive bins in depth, i.e., over a range of 0.05 mm. The averaged dose distribution was fitted to a bivariate Gaussian function to locate the position of the dose maximum. The dose calculated for each simulation was defined as the average dose over a circular disk of 2.5 mm radius centred at the beam centre.

2.2.2 Characterization of dose enhancement ratio

The dependence of the DER on the magnetic field strength and orientation as well as on the proton energy at the PMMA-air interface was systematically investigated by performing a set of simulations with the same geometrical configurations of the setups (A) and (B) together with the following simplifications.

The proton beam was simulated as a mono-energetic beam with a circular cross-section starting at the collimator. The initial proton energies were chosen such that the mean proton energies at the PMMA-air interface in setup (B) result in 50, 100, 150 and 200 MeV. The magnetic field was modelled as an ideal dipole field in vertical direction (transverse to the proton beam) with field strengths of 0.35, 0.5, 1.0, 1.5, and 3.0 T. In addition, the case of a 1.0 T magnetic field parallel to the proton beam was considered to study the dependence of the DER on the field orientation. The magnetic field extended from 50 mm upstream to 100 mm downstream of the PMMA-air interface in setup (B).

The same threshold for production of secondary electrons, scoring method, and data analysis procedure as used in the simulation of the irradiation experiment were applied to characterise the DER.

3. Results

3.1. Dose response of EBT3 films in a magnetic field

A linear dose response of the EBT3 films to proton irradiation was measured ($R^2 \geq 0.994$) in a dose range from 1 to 11 Gy (Figure 2) with and without magnetic field. The film dose as function of MU did not show any significant influence on whether the orientation of the short film side was parallel or perpendicular to the direction of the magnetic field. However, a reproducible and significant decrease of the dose response of about 3% was measured for films placed in the magnetic field compared to measurements without magnetic field. The relative decrease of the dose response in the magnetic field was found to be independent of the absolute dose, allowing the use of EBT3 films for relative dose measurements in the presence of a magnetic field.

3.2. Irradiation experiments and validation of computer simulations

In a 0.92 T transverse magnetic field, the normalised dose of a 200 MeV proton beam in PMMA measured at a distance of 0.156 mm from the air interface was 1.018 ± 0.003, i.e., significantly larger ($p<0.001$) by (1.8 ± 0.3)% than the dose at the same depth when no air interface was present. Also, the normalised dose with magnetic field measured at a distance of 0.156 mm to the air interface was significantly larger ($p<0.001$) compared to the normalised dose without magnetic field (Figure 3). These findings were confirmed by the repetition of the experiment.

The simulated normalised dose as a function of distance to the PMMA-air interface for the irradiation experiment was in agreement with the measured normalised dose both with and without magnetic field. With magnetic field, the normalised dose was found to increase by at least 6% within the last millimetre proximal to the PMMA-air interface (Figure 3). Without magnetic field, the simulated normalised dose in the same region decreased by at least 2% towards the interface. The measured DERs at 0.156 mm and 0.467 mm from the interface were highly significant ($p<0.00001$) for both experiment repetitions. The simulated DER in the 0.92 T magnetic field increased from about 1 to 1.075 over a distance of 1 mm to 0.025 mm from the interface (Figure 4).

An excellent agreement was found between the normalised dose pooled from the experiment runs Exp1 and Exp2 and the computer simulation, with a relative difference of about 0.15%. This agreement was observed for all experimental settings: with and without magnetic field and at the two measurement points at a depth of 0.156 mm and 0.467 mm from the air interface. Accordingly, the pooled experimental DER data also agreed well with the simulations (Figure 4) and the simulation setup could be considered to be validated to perform further simulations, covering different (clinically relevant) magnetic field strengths and orientations, as well as proton beam energies.

3.3. Variation of simulation parameters: magnetic field strength, orientation, proton energy and voxel size

The normalised dose deposited by a 200 MeV proton beam in PMMA close to an air interface was calculated with and without the presence of a homogeneous 1.0 T magnetic field oriented parallel or transverse to the proton beam (Figure 5a). For a transverse field orientation, the normalised dose increased with decreasing distance to the air interface, which is in accordance with the irradiation experiments. For a parallel field orientation, however, the normalised dose decreased by less than 0.5% over the last 1 mm towards the air interface. Evidently, the calculated DER is significantly larger for the transverse field orientation than for the parallel field orientation (Figure 5b). The small increase in DER for the parallel field orientation (< 1% compared to 7% for the transverse field) originated from the more pronounced decrease in normalised dose without magnetic field close to the air.

The calculated maximum DER in a transverse field increased with magnetic field strength, from 2.6% to 8.2% for 0.35 and 1.5 T, respectively (Figure 6a). However, the increase of the DER between 1.0 T and 1.5 T was small (≤ 0.5%). A further increase in magnetic field strength from 1.5 T to 3.0 T showed an insignificant decrease in the DER, indicating a saturating effect (Figure 7). A decrease in the proton energy from 200 to 50 MeV resulted in a decrease in the maximum DER from 7.6% to 3.2%, respectively (Figure 6b). The shape of the curve (on the logarithmic scale) remained similar for the different energies. However, with decreasing proton energy, the entire DER curves were effectively shifted toward smaller distances. To

visualise this proton energy dependent shift, all distances (i.e., x values of DER curves) were scaled with the factor f = ($\bar{E}$-E_0) / (E-E_0), with E being the proton energy of the scaled curve, $\bar{E}$ = 200 MeV, and E_0 = 25 MeV an energy offset. The scaled curves resembled the DER curve for 200 MeV protons except for values around their DER maximum (Supplement Figure 11).

For proton energies below 100 MeV as well as for magnetic field strengths below 0.5 T), a DER greater than 1% was only found within 0.1 mm from the air interface. Also, all studied scenarios suggested that there was no dose enhancement at distances larger than 1 mm from the air interface. The strong dependence of the DER on the distance to the air interface implied a strong dependence of the maximum DER on the dose voxel size (Table 1). For clinically established voxel lengths of 0.5 and 1.0 mm the maximum DER values were smaller than 3% and 1.5%, respectively, for all parameters considered in this study.

4. Discussion

The complete integration of MRI and proton therapy results in dose distributions that are affected by the strong static magnetic field of the MR scanner. For a setup where the incident beam is perpendicular to the magnetic field, the beam trajectory is deflected by the Lorentz force with energy-dependent lateral Bragg peak displacements of a few millimetres up to centimetres (Wolf and Bortfeld 2012, Schellhammer *et al* 2018) for field strengths in the order of 1 T. Second, in this work, the electron return effect for proton beams in a transverse magnetic field was demonstrated experimentally and quantified in detail by Monte Carlo simulations for clinically relevant conditions. The measured dose enhancement at a tissue-air interface is significant and predictable by simulations. The ERE was found to be limited to within 1 mm from the air interface under clinically relevant magnetic field configurations and proton beam energies. Furthermore, the dose response of EBT3 films irradiated with a proton beam in a strong magnetic field (0.92 T) was studied experimentally showing a linear dose response with an under-response of about 3% compared to no field.

The trajectories of secondary electrons produced by the ionizing radiation–relevant for DNA damage–are influenced by the strong magnetic field. While slowing down, the electrons move on orbits with a decreasing radius around the direction of the magnetic field depending on the electron velocity and magnetic field strength. In proton therapy, most of these electrons have low kinetic energies (median energy about 15 eV, Supplement Figure 12) and short ranges in tissue and therefore, no major effect on the dose distribution is expected. In air, however, the electron ranges are much longer (due to the low density of air) and some electrons at a tissue-air interface possess sufficient energy to exit the tissue and travel, due to the Lorentz force, on a half cycle through air back into the tissue. The penetration depth of a returning electron – and hence the impact of the ERE – increases with the remaining energy when re-entering the tissue. Both, a higher proton beam energy and magnetic field strength at the interface result in on average increasing energies of the returning electrons. For proton beams of 100 – 200 MeV, the mean energy of the secondary electrons is about 70 eV, while it is approximately 1 MeV and therefore much higher for a 6 MV photon beam (Raaijmakers *et al* 2008). Accordingly, a strikingly more pronounced DER at a tissue-air interface can be observed for MRXT compared to MRPT.

For a magnetic field in parallel to the proton beam, the ERE vanishes due to the minimum impact of the Lorentz force while the dose fall-off in the tissue near the air interface is less pronounced. Studies related to MRXT in low-density tissue reported the same effect for inline magnetic fields on the dose distribution (Oborn *et al* 2017b, Schrenk *et al* 2017) , though, in a more pronounced extent than for proton beams.

So far, no measurement data for the ERE of proton beams have been available in the literature. The current findings on the ERE are in accordance with a recent simulation study in a phantom geometry (Fuchs *et al* 2017). The authors reported on the analysis of simulated secondary charged particles of ion beams in magnetic fields and found that only electrons contributed non-negligibly to the dose distribution. Using a voxel size of $0.5\times0.5\times0.5$ mm^3, they concluded that the impact on the dose (averaged over the volume of a voxel) was found to be below 2% for the highest energies (about 150 MeV protons at the air interface) and magnetic fields (3 T) evaluated. Earlier, Raaymakers et al. concluded that the impact of the ERE caused by a transverse 0.5 T

magnetic field on the dose distribution for proton therapy is negligible (Raaymakers *et al* 2008). In their simulations, they could not resolve any effect at tissue-air interfaces of the magnetic field on the dose distribution of a 90 MeV proton beam on a voxel length of 1 mm in beam direction. For their settings, our results, as given in Table 1, suggest a DER of only few per mill. Based on their assumption that the energy distribution of the secondary electrons is independent of the proton energy they stated that their conclusions are valid for all practical proton energies. In contrast to this, the present study shows a systematic dependence of the ERE on the proton energy at the air interface. While the mean energy of the secondary electrons only varies slowly with proton energy, the maximum energy of the secondary electrons increases approximately linearly with proton energy (ICRU Report 49 1993), e.g., from 0.11 MeV to 0.48 MeV for 50 MeV and 200 MeV protons, respectively. The higher electron energies result in larger electron ranges and, hence, a more pronounced DER also at larger distances from the air interface.

In a Monte Carlo based proton treatment planning study (Moteabbed *et al* 2014), the impact of a transverse 0.5 and 1.5 T magnetic field was analysed for nine patients covering six different treatment sites including one skull base and two lung cases. No voxel size was specified. The ERE was found to be negligible in the analysis of global dose-volume histograms. Since the ERE in proton therapy is expected to change the dose primarily in cell layers adjacent to an air interface, a treatment planning system that is able to describe the ERE correctly has to support small voxel sizes and a detailed description of electron trajectories. Also, the ERE is expected to be more pronounced for lung or head and neck patients with air-filled cavities compared to brain and prostate treatments with less density inhomogeneity. For MRXT, a transverse magnetic field can significantly change the dose on tissue interfaces when not included in plan optimization (Chen *et al* 2016). However, considering the ERE during plan optimization allows for a substantial reduction or even for an elimination of these dose changes.

The introduction of MRXT has led to special attention regarding the impact of a magnetic field on radiation dose measurements. For EBT2 films irradiated with a ^{60}Co MRXT system (B = 0.35 T), a considerable under-response and a dependence on the dominant orientation of the monomer crystals relative to the magnetic field were

observed (Reynoso *et al* 2016). Recently, small but significant changes of the radiochromic EBT3 film response to 6 MV photons on the order of a 2% decrease were reported for 0.35 and 1.42 T (Delfs *et al* 2018). In our study, EBT3 films irradiated with a proton beam in a 0.92 T magnetic field showed an under-response of similar magnitude (about 3%). Notably, the EBT3 dose response to proton irradiation in a magnetic field was linear and no dependence on the film orientation relative to the magnetic field direction during irradiation was found both in accordance with (Delfs *et al* 2018).

Absolute proton dose measurement based on film dosimetry is known to be associated with considerable uncertainties and would require a magnetic field-dependent calibration of the EBT3 films for proton irradiation. On the other hand, the observed linear dose response of EBT3 films in the presence of a magnetic field makes them suitable for relative dose measurements, as also found by (Delfs *et al* 2018). Therefore, it appears adequate to study the DER as described in Eq. (2), i.e., by normalizing dose values from measurement condition in setup (B) by those from the reference measurements in setup (A). Simulations of absolute dose values in reference setup (A) with and without magnetic field confirmed the assumption that they do not differ significantly (cf. Figure 10 in the supplement). Hence, the differences in measured dose for setup (A) with and without magnetic field could be first, attributed to the different dose response in a magnetic field and second, used to minimise the impact of this effect on the dose measured in setup (B) by normalization to the respective reference dose values. In addition, the normalization mitigated other possible systematic differences with and without magnetic field caused by, e.g., the deflection of the proton beam and small changes in the energy spectrum of protons traversing the film that could have a small impact on the absolute dose distribution.

The range of magnetic field strengths in this study was limited to an interval between 0 and 3 T which was considered to be clinically relevant for an integration of MRI and proton therapy. First, it comprises the magnetic field strengths of currently available MRXT devices and second, for even higher field strengths effects, such as the lateral displacement of the Bragg peak, may become too large. Similarly, proton energies were limited to an interval up to 200 MeV, which is an energy range that typically occurs inside patients. A systematic reduction of the air gap to sizes smaller

than the maximum gyration radius of the electrons in order to quantify the impact on the DER was beyond the scope of this study, in particular, since the radii of the electron trajectories vary with proton energy and with magnetic field strength.

Considerable changes of the dose response of ionization chambers have been found for MRXT caused by magnetic field induced alterations of the electron trajectories in a small air cavity. These changes were non-linear and depended on the field strength and orientation of the magnetic field relative to the photon beam (Meijsing *et al* 2009, Spindeldreier *et al* 2017). A comparable study that is dedicated to the dosimetry of proton beams with air-filled ionization chambers in strong magnetic fields is still missing. However, it is absolutely necessary to quantify the impact of the ERE before using these devices for patient dosimetry in MRPT.

5. Conclusion

For proton beams in a transverse magnetic field significant dose enhancement was demonstrated experimentally at a PMMA-air interface due to the ERE. Systematic computer simulations show that the dose enhancement is predictable and depends on the magnetic field strength, field orientation, proton energy and distance to the interface. Under clinically relevant conditions, the maximum proton dose enhancement is expected to be limited to about 10% within the first 1 mm from the air interface. This is significantly less than the 40% local dose enhancement, which has been reported for photons in a transverse magnetic field. However, the impact of strong magnetic fields on proton dosimetry with air-filled ionisation chambers and on porous tissue (e.g. lung parenchyma) irradiation remains to be established.

Tables

Table 1: Calculated dose enhancement ratio (DER) in a voxel directly adjacent to the air interface for different magnetic field strengths, proton energies, and voxel lengths.

B field	Energy	DER		
[T]	[MeV]	0.05 mm	0.50 mm	1.00 mm
0.35	200	1.026	1.004	1.002
0.5	200	1.044	1.009	1.004
1.0	200	1.076	1.023	1.013
1.5	200	1.082	1.026	1.014
3.0	200	1.080	1.026	1.014
1.0	50	1.032	1.004	1.002
1.0	100	1.058	1.011	1.005
1.0	150	1.070	1.018	1.009
1.0	200	1.076	1.023	1.013

Figures

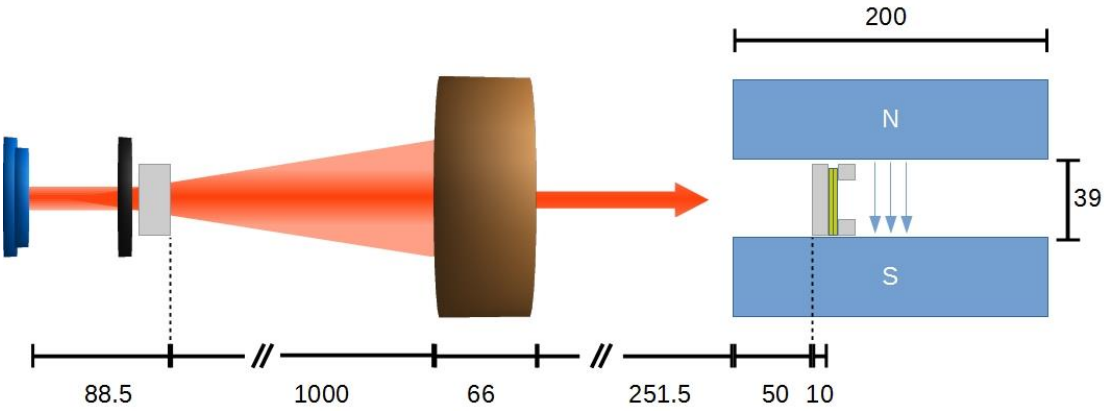

Figure 1: Schematic view of setup for the irradiation experiment. The collimated proton beam enters from the left into the vertical field of the permanent magnet. Two EBT3 films are attached to a vertically placed slab of PMMA, which corresponds to setup (B). In setup (A), the film is sandwiched between two PMMA slabs (not shown). All dimensions are given in mm.

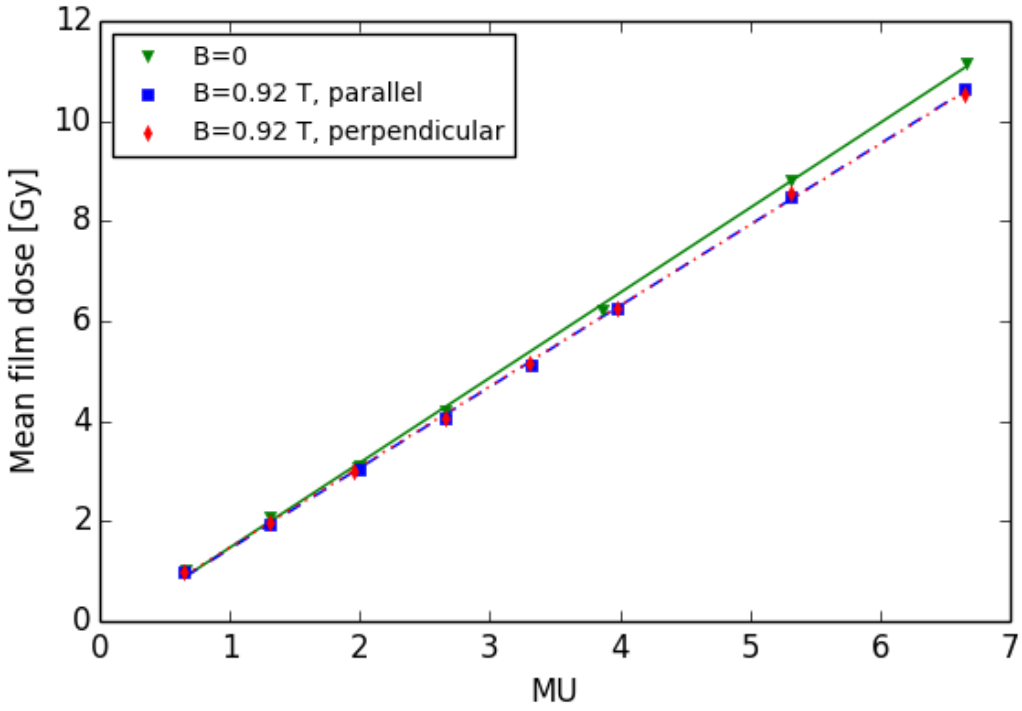

Figure 2: Mean dose over a circular disk of 2.5 mm radius centred at the beam centre measured with EBT3 films as function of the applied proton beam monitor units (MU). The film dose was measured without (*B* = 0 T) and with (B = 0.92 T) the field of the permanent magnet. Two film orientations were used: monomers parallel or perpendicular to the magnetic field direction. The lines represent linear regression curves for no magnetic field (solid line), parallel magnetic field (dashed line) and perpendicular magnetic field (dotted line).

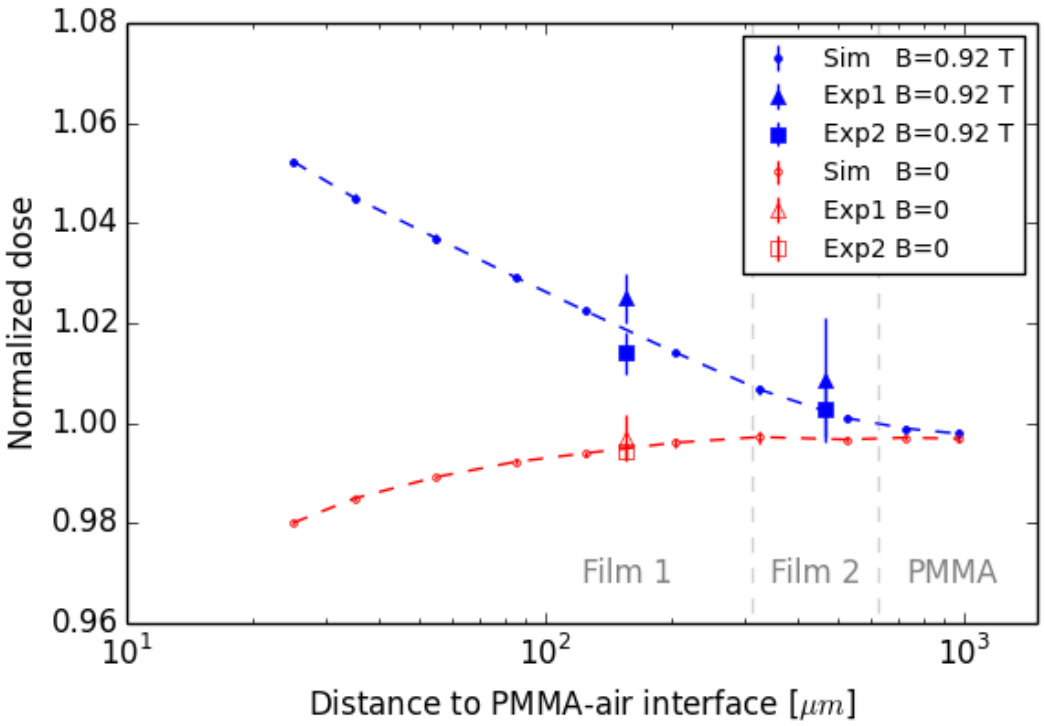

Figure 3: Measured and simulated normalised dose for a 200 MeV proton beam in PMMA and in EBT3 films without (red open symbols) and with (blue closed symbols) 0.92 T magnetic field as function of the distance to the PMMA-air interface. Vertical dashed lines indicate the borders between the films and the proximal PMMA slab.

Sim = computer simulation; Exp1 = irradiation experiment 'Exp1'; Exp2 = irradiation experiment 'Exp2'.

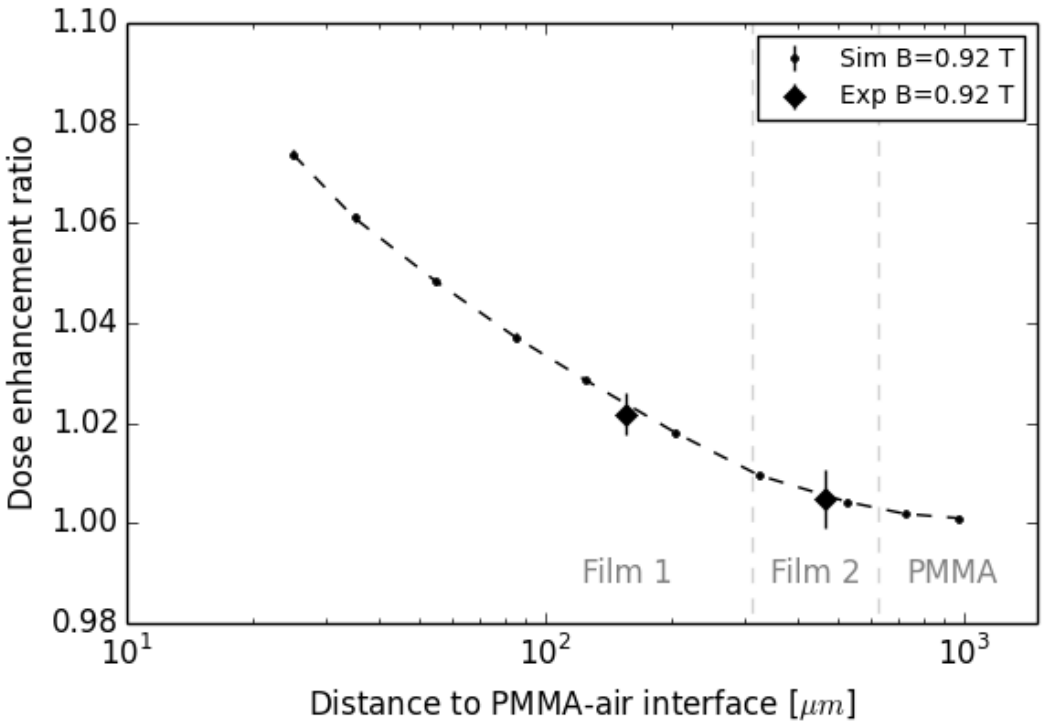

Figure 4: Measured (diamond symbol) and simulated (dashed line) dose enhancement ratio for a 200 MeV proton beam in PMMA and EBT3 film in a 0.92 T magnetic field as a function of the distance to the PMMA-air interface. Vertical dashed lines indicate the borders between the films and the proximal PMMA slab.

Sim = computer simulation; Exp = irradiation experiment.

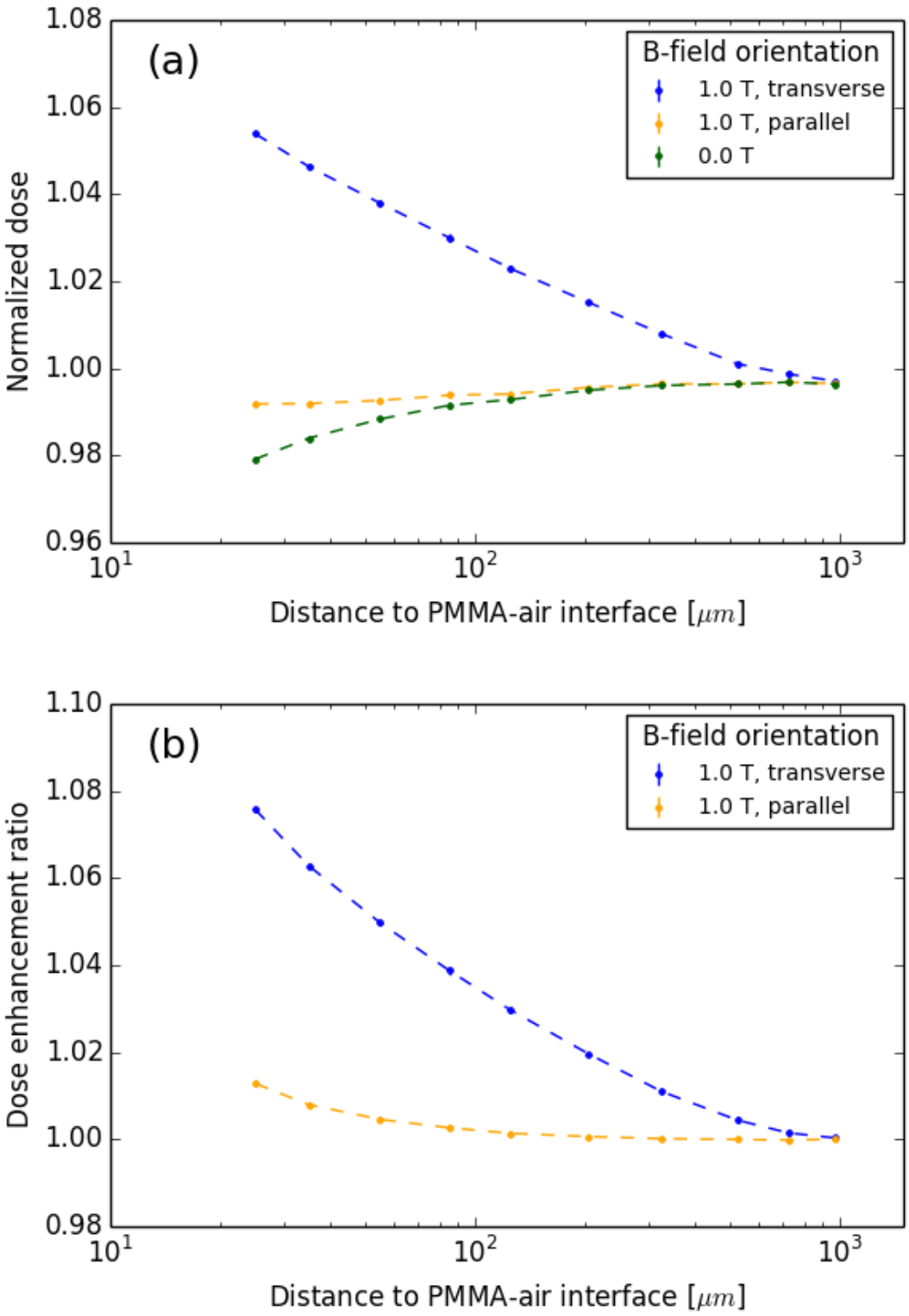

Figure 5: Simulated (a) normalised dose and (b) dose enhancement ratio for a 200 MeV proton beam as function of the distance to the PMMA-air interface for three magnetic field settings: no field, 1.0 T parallel to beam direction, and 1.0 T transverse to beam direction.

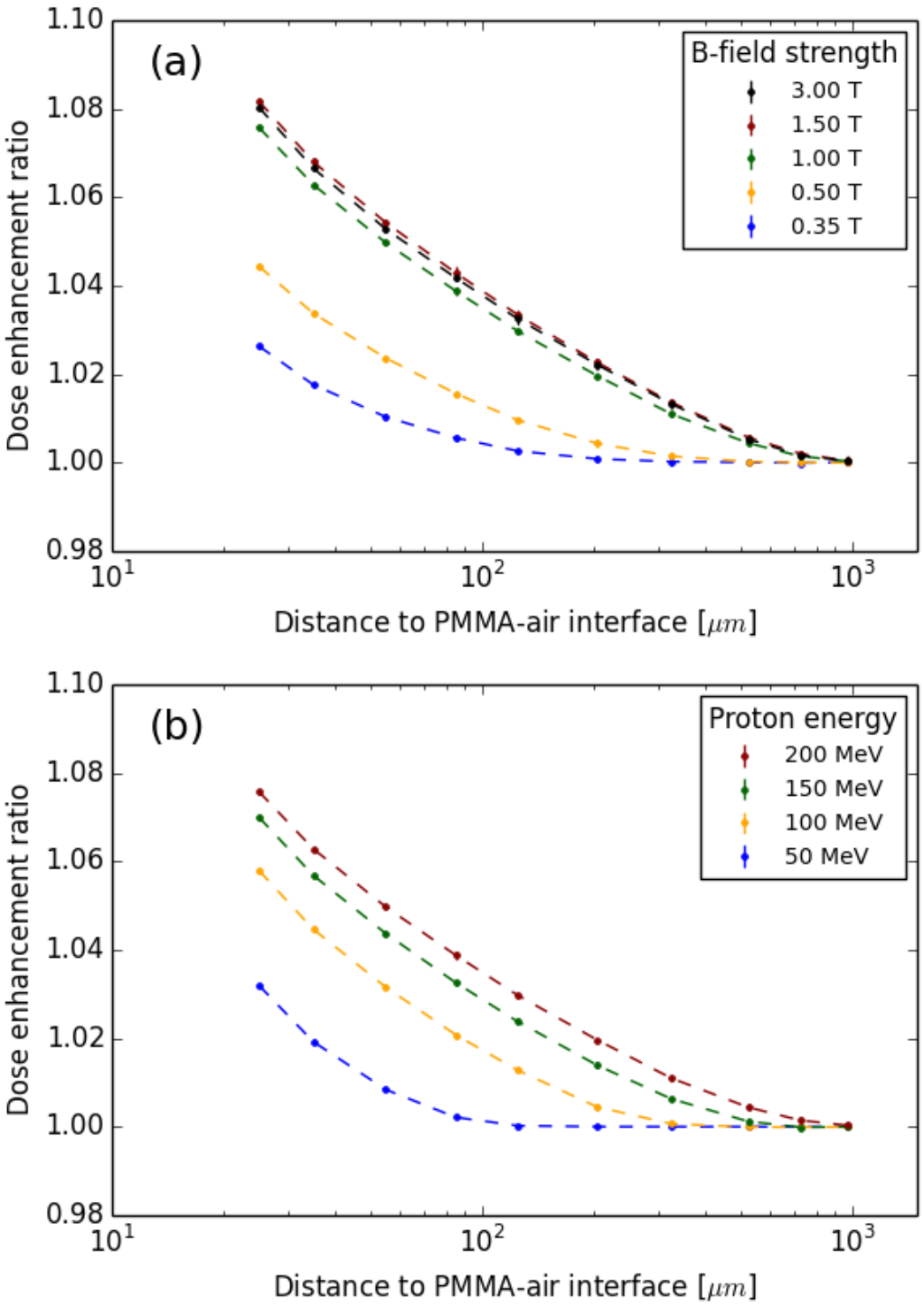

Figure 6: Simulated dose enhancement ratio as function of the distance to the PMMA-air interface in a transverse magnetic field for (a) a 200 MeV proton beam and different magnetic field strengths, and (b) a 1.0 T magnetic field and different proton beam energies.

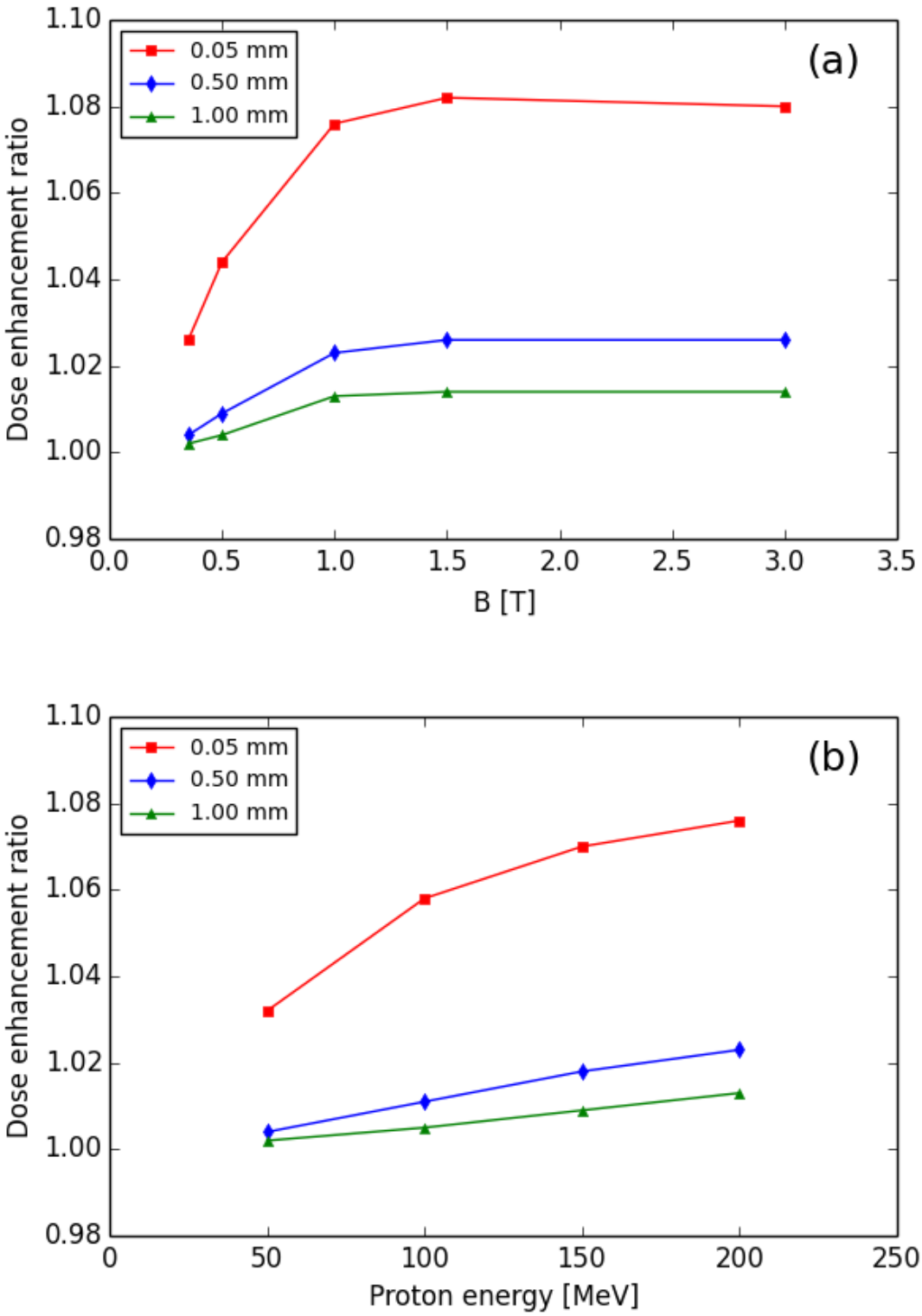

Figure 7: Dose enhancement ratio averaged in a voxel directly adjacent to the PMMA-air interface for three different voxel lengths, as function of (a) the magnetic field strength and (b) the proton beam energy.

Supplementary data

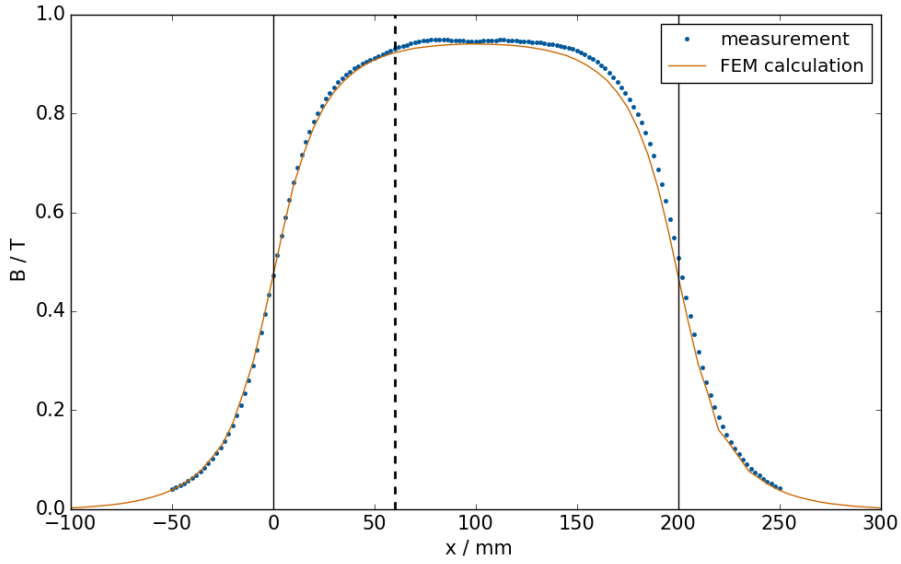

Figure 8: Measured and calculated vertical magnetic field component along the beam axis in the central plane of the permanent magnet's magnetic field (Gantz 2017). The vertical dashed and solid lines indicate the position of the EBT3 film and the extension of the magnet assembly, respectively.

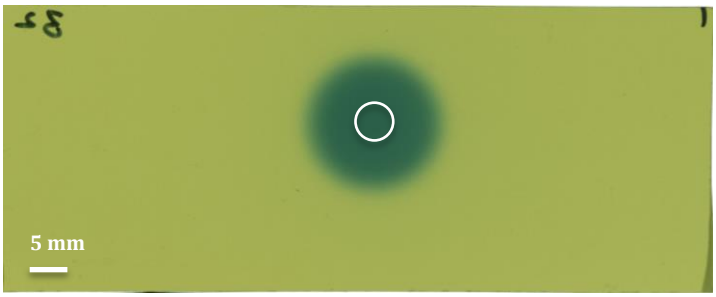

Figure 9: Scan of EBT3 film exposed to a cylindrical proton beam with about 8 Gy. The black line (upper right corner) denotes the monomer orientation (parallel to the film's short side). The white circle indicates the circular disk of 2.5 mm radius centred at the beam centre that is used for dose evaluation.

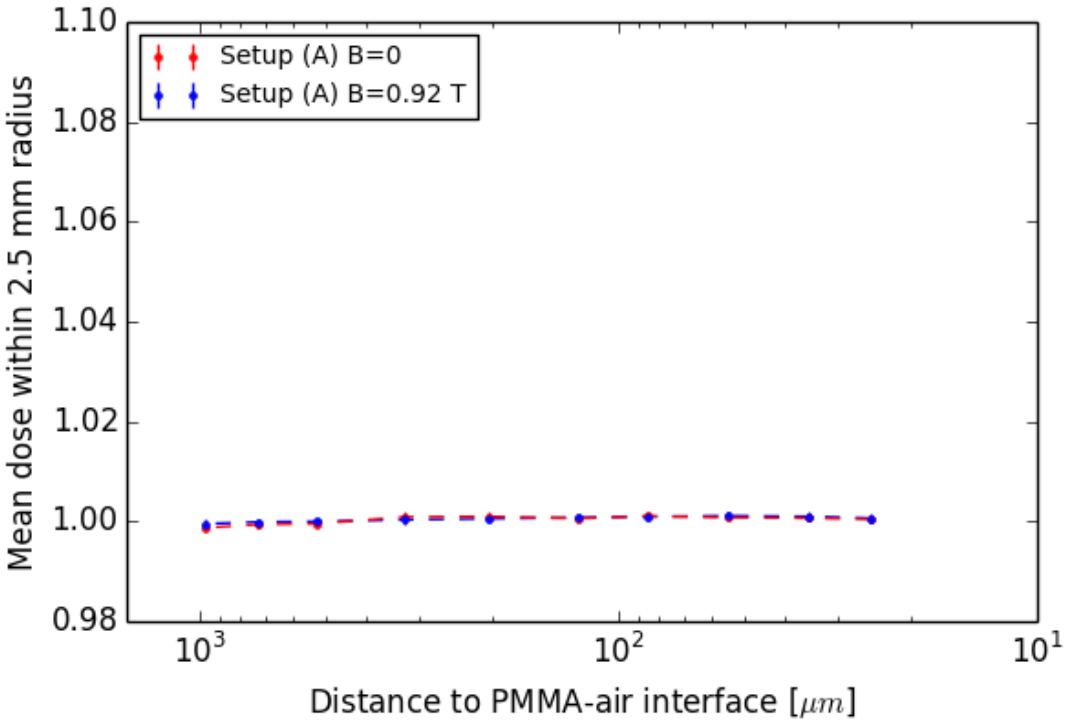

Figure 10: Mean dose within a 2.5 mm radius around the center of a 200 MeV proton beam spot simulated for the reference setup (A) with and without magnet. Both curves are normalised to the same dose value, i.e., the mean dose without magnet at 0.025 mm distance from the interface.

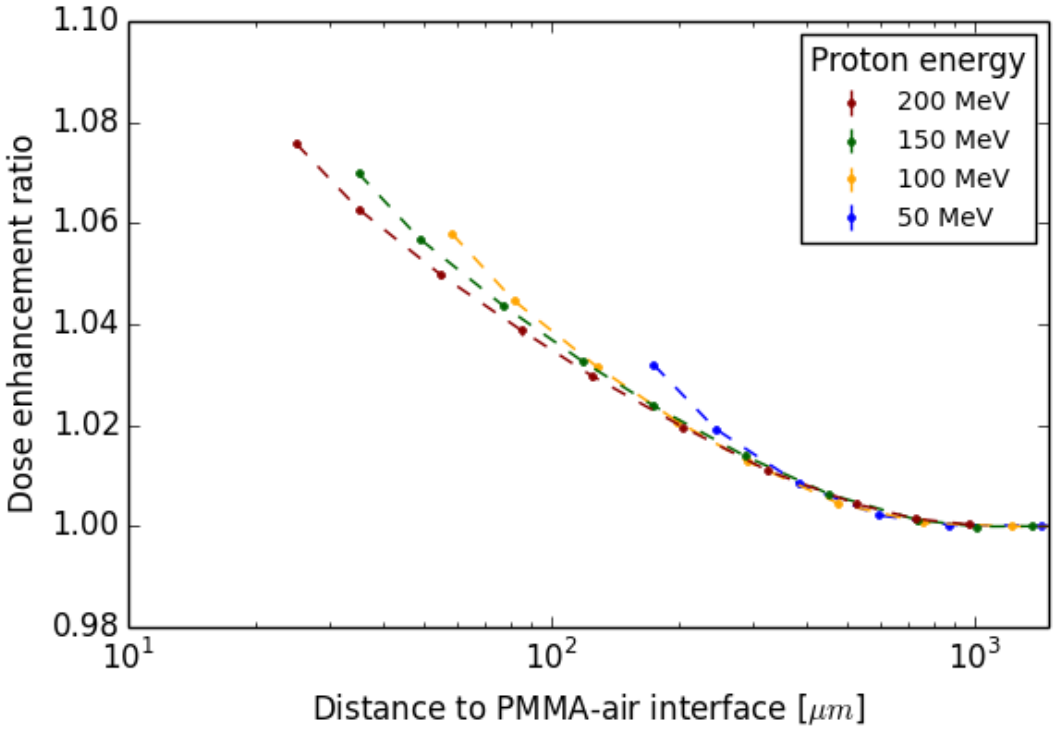

Figure 11: Simulated dose enhancement ratio as function of the distance to the PMMA-air interface in a transverse magnetic field for a 1.0 T magnetic field and different proton beam energies. Same data as in Figure 6 but all distance values are scaled by the factor ($\bar{E}$-E_0) / (E-E_0), with E being the proton energy, $\bar{E}$ = 200 MeV, and E_0 = 25 MeV.

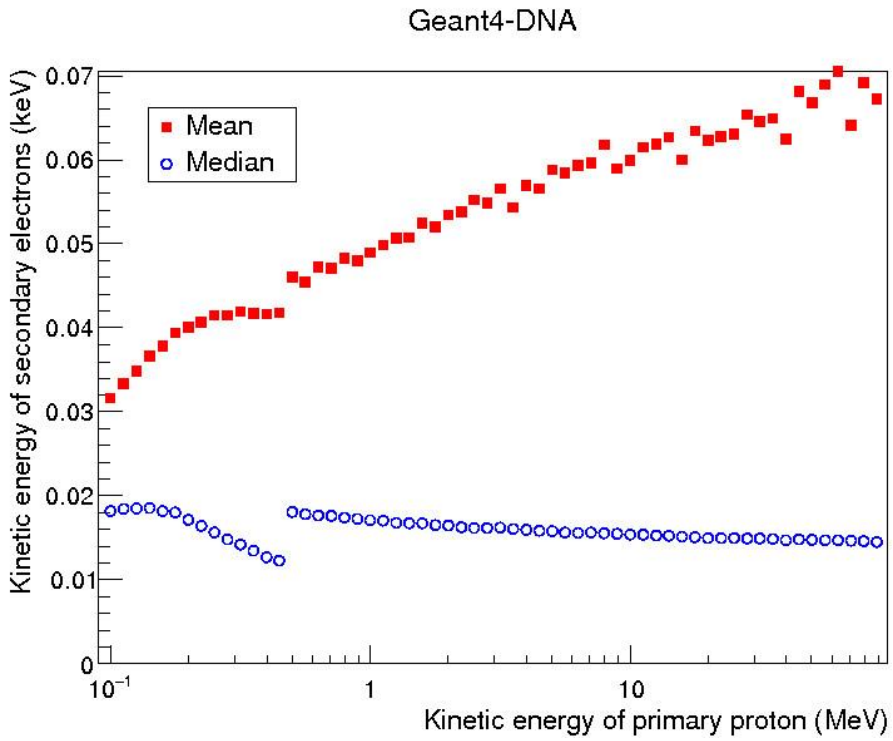

Figure 12: Calculated kinetic energy of secondary electrons in water produced by monoenergetic protons. Simulations were performed with the Monte Carlo software Geant4-DNA.

References

Agostinelli S, Allison J, Amako K, Apostolakis J, Araujo H, Arce P, Asai M, Axen D, Banerjee S, Barrand G, Behner F, Bellagamba L, Boudreau J, Broglia L, Brunengo A, Burkhardt H, Chauvie S, Chuma J, Chytracek R, Cooperman G, Cosmo G, Degtyarenko P, Dell'Acqua A, Depaola G, Dietrich D, Enami R, Feliciello A, Ferguson C, Fesefeldt H, Folger G, Foppiano F, Forti A, Garelli S, Giani S, Giannitrapani R, Gibin D, Gómez Cadenas J J, González I, Gracia Abril G, Greeniaus G, Greiner W, Grichine V, Grossheim A, Guatelli S, Gumplinger P, Hamatsu R, Hashimoto K, Hasui H, Heikkinen A, Howard A, Ivanchenko V, Johnson A, Jones F W, Kallenbach J, Kanaya N, Kawabata M, Kawabata Y, Kawaguti M, Kelner S, Kent P, Kimura A, Kodama T, Kokoulin R, Kossov M, Kurashige H, Lamanna E, Lampén T, Lara V, Lefebure V, Lei F, Liendl M, Lockman W, Longo F, Magni S, Maire M, Medernach E, Minamimoto K, Mora de Freitas P, Morita Y, Murakami K, Nagamatu M, Nartallo R, Nieminen P, Nishimura T, Ohtsubo K, Okamura M, O'Neale S, Oohata Y, Paech K, Perl J, Pfeiffer A, Pia M G, Ranjard F, Rybin A, Sadilov S, Di Salvo E, Santin G, Sasaki T, et al 2003 Geant4—a simulation toolkit *Nucl. Instrum. Methods Phys. Res. Sect. Accel. Spectrometers Detect. Assoc. Equip.* **506** 250–303

Allison J, Amako K, Apostolakis J, Araujo H, Arce Dubois P, Asai M, Barrand G, Capra R, Chauvie S, Chytracek R, Cirrone G A ., Cooperman G, Cosmo G, Cuttone G, Daquino G G, Donszelmann M, Dressel M, Folger G, Foppiano F, Generowicz J, Grichine V, Guatelli S, Gumplinger P, Heikkinen A, Hrivnacova I, Howard A, Incerti S, Ivanchenko V, Johnson T, Jones F, Koi T, Kokoulin R, Kossov M, Kurashige H, Lara V, Larsson S, Lei F, Link O, Longo F, Maire M, Mantero A, Mascialino B, McLaren I, Mendez Lorenzo P, Minamimoto K, Murakami K, Nieminen P, Pandola L, Parlati S, Peralta L, Perl J, Pfeiffer A, Pia M G, Ribon A, Rodrigues P, Russo G, Sadilov S, Santin G, Sasaki T, Smith D, Starkov N, Tanaka S, Tcherniaev E, Tome B, Trindade A, Truscott P, Urban L, Verderi M, Walkden A, Wellisch J P, Williams D C, Wright D and Yoshida H 2006 Geant4 developments and applications *IEEE Trans. Nucl. Sci.* **53** 270–8

Beyreuther E 2018 Research facility for radiobiological studies at the University Proton Therapy Dresden *Int. J. Part. Ther.* **in press**

Chen X, Prior P, Chen G-P, Schultz C J and Li X A 2016 Technical Note: Dose effects of 1.5 T transverse magnetic field on tissue interfaces in MRI-guided radiotherapy *Med. Phys.* **43** 4797–802

Delfs B, Schoenfeld A A, Poppinga D, Kapsch R-P, Jiang P, Harder D, Björn Poppe and Looe H K 2018 Magnetic fields are causing small, but significant changes of the radiochromic EBT3 film response to 6 MV photons *Phys. Med. Biol.* **63** 035028

Fuchs H, Moser P, Gröschl M and Georg D 2017 Magnetic field effects on particle beams and their implications for dose calculation in MR-guided particle therapy *Med. Phys.* **44** 1149–56

Gantz S 2017 *Characterization of the magnetic field of a 0.95 T permanent dipole magnet and experimental validation of proton beam deflection in a magnetic field within tissue-equivalent material.* Master's Thesis (Dresden: Technische Universität Dresden)

ICRU Report 49 1993 *Stopping powers and ranges for protons and alpha particles* (Bethesda, Maryland: International Commission on Radiation Units and Measurements)

Kurz C, Landry G, Resch A F, Dedes G, Kamp F, Ganswindt U, Claus Belka, Raaymakers B W and Parodi K 2017 A Monte-Carlo study to assess the effect of 1.5 T magnetic fields on the overall robustness of pencil-beam scanning proton radiotherapy plans for prostate cancer *Phys. Med. Biol.* **62** 8470

Meijsing I, Raaymakers B W, Raaijmakers A J E, Kok J G M, Hogeweg L, Liu B and Lagendijk J J W 2009 Dosimetry for the MRI accelerator: the impact of a magnetic field on the response of a Farmer NE2571 ionization chamber *Phys. Med. Biol.* **54** 2993

Moteabbed M, Schuemann J and Paganetti H 2014 Dosimetric feasibility of real-time MRI-guided proton therapy *Med. Phys.* **41** n/a-n/a

Mutic S and Dempsey J F 2014 The ViewRay System: Magnetic Resonance–Guided and Controlled Radiotherapy *Semin. Radiat. Oncol.* **24** 196–9

Oborn B M, Gargett M A, Causer T J, Alnaghy S J, Hardcastle N, Metcalfe P E and Keall P J 2017 Experimental verification of dose enhancement effects in a lung phantom from inline magnetic fields *Radiother. Oncol.* **0** Online: http://www.thegreenjournal.com/article/S0167-8140(17)32579-3/fulltext

Perl J, Shin J, Schumann J, Faddegon B and Paganetti H 2012 TOPAS: An innovative proton Monte Carlo platform for research and clinical applications *Med. Phys.* **39** 6818–37

Raaijmakers A J E, Raaymakers B W and Lagendijk J J W 2005 Integrating a MRI scanner with a 6 MV radiotherapy accelerator: dose increase at tissue–air interfaces in a lateral magnetic field due to returning electrons *Phys. Med. Biol.* **50** 1363

Raaijmakers A J E, Raaymakers B W and Lagendijk J J W 2008 Magnetic-field-induced dose effects in MR-guided radiotherapy systems: dependence on the magnetic field strength *Phys. Med. Biol.* **53** 909

Raaymakers B W, Jürgenliemk-Schulz I M, Bol G H, Glitzner M, Kotte A N T J, Asselen B van, Boer J C J de, Bluemink J J, Hackett S L, Moerland M A, Woodings S J, Wolthaus J W H, Zijp H M van, Philippens M E P, R Tijssen, Kok J G M, Breugel E N de G, Kiekebosch I, Meijers L T C, Nomden C N, Sikkes G G, Doornaert P A H, Eppinga W S C, Kasperts N, Kerkmeijer L G W, Tersteeg J H A, Brown K J, Pais B, Woodhead P and Lagendijk J J W 2017 First patients treated with a 1.5 T MRI-Linac: clinical proof of concept of a high-precision, high-field MRI guided radiotherapy treatment *Phys. Med. Biol.* **62** L41

Raaymakers B W, Raaijmakers A J E and Lagendijk J J W 2008 Feasibility of MRI guided proton therapy: magnetic field dose effects *Phys. Med. Biol.* **53** 5615

Reynoso F J, Curcuru A, Green O, Mutic S, Das I J and Santanam L 2016 Technical Note: Magnetic field effects on Gafchromic-film response in MR-IGRT *Med. Phys.* **43** 6552–6

Schellhammer S M, Gantz S, Lühr A, Oborn B M, Bussmann M and Hoffmann A L 2018 Technical Note: Experimental verification of magnetic field induced beam deflection and Bragg peak displacement for MR-integrated proton therapy *Med. Phys.* **0** Online: https://aapm.onlinelibrary.wiley.com/doi/10.1002/mp.12961

Schellhammer S M and Hoffmann A L 2017 Prediction and compensation of magnetic beam deflection in MR-integrated proton therapy: a method optimized regarding accuracy, versatility and speed *Phys. Med. Biol.* **62** 1548

Schrenk O, Spindeldreier C K, Burigo L N, Hoerner-Rieber J and Pfaffenberger A 2017 Effects of magnetic field orientation and strength on the treatment planning of nonsmall cell lung cancer *Med. Phys.* **44** 6621–31

Spindeldreier C K, Schrenk O, Bakenecker A, Kawrakow I, Burigo L, Karger C P, Greilich S and Pfaffenberger A 2017 Radiation dosimetry in magnetic fields with Farmer-type ionization chambers: determination of magnetic field correction factors for different magnetic field strengths and field orientations *Phys. Med. Biol.* **62** 6708

Wolf R and Bortfeld T 2012 An analytical solution to proton Bragg peak deflection in a magnetic field *Phys. Med. Biol.* **57** N329–37